JOURNAL OF Materials CHEMISTRY

Colloidal zeolites and zeolite membranes†

S. Kallus,[a] J.-M. Condre,[a] A. Hahn,[b] G. Golemme,[c] C. Algieri,[d] Ph. Dieudonné,[e] P. Timmins[f] and J. D. F. Ramsay*[a]

[a]*CNRS, Institut Européen des Membranes, 1919 Route de Mende, 34293 Montpellier, France. E-mail: ramsay@crit.univ-montp2.fr*
[b]*Institute for Inorganic Chemistry and Analytical Chemistry, Johannes Gutenberg University, Mainz, Germany*
[c]*Dipartimento di Ingegneria Chimica e dei Materiali, Universite Calabria, Rende, Italy*
[d]*Instituto di Ricerca su Membrane e Modellistia di Reattori Chimici-CNR, Rende, Italy*
[e]*GDPC, UMR 5581, Université de Montpellier II, 34095 Montpellier, France*
[f]*Institut Laue Langevin, 38042 Grenoble, France*

Received 30th April 2002, Accepted 21st June 2002
First published as an Advance Article on the web 3rd October 2002

The synthesis of zeolite membranes and thin films using the secondary growth process is briefly described. In this process colloidal zeolite particles (sols) are prepared hydrothermally and then subsequently deposited on substrates to produce uniform layers of controlled thickness. In order to optimise this process, an understanding of the nature of the sols and an insight into the structure of the consolidated layer so formed, is required. Such studies are illustrated here with silicalite and zeolite A. The formation and growth of silicalite sols has been investigated *in situ* by small angle neutron scattering (SANS). SANS measurements on sols at progressively higher concentrations have provided details of the colloid interactions which lead to zeolite gel-layer structures which are uniform and free of defects. Several techniques (XRD, small angle X-ray scattering (SAXS), and nitrogen adsorption isotherms) have also been used to characterize colloidal species extracted by ultracentrifugation at progressive stages from solutions during the hydrothermal synthesis of zeolite LTA.

Introduction

Zeolites are in general crystalline alumino-silicate or silicate materials which have a highly regular and open microporous (<2 nm) structure[1] formed by a three-dimensional network of SiO_4 and AlO_4 tetrahedra. The tetrahedra are linked together to give cages connected by pore openings of defined size; depending on the structural type, the pore sizes range from $\sim$0.3 to $\sim$1 nm. Almost a hundred different structural types of zeolite are known. Each of these has a distinct pore size, shape and interconnectivity. Because of these properties, zeolites can interact very selectively with adsorbed molecules. These exceptional properties have led to numerous technical applications for zeolites in bulk powder form (heterogeneous catalysis, gas separation, adsorption). However, more recently there has been a surge of interest in the potential applications of thin films or membranes of zeolites. These include highly selective separation membranes,[2,3] sensors, conductors, and optoelectronic devices.[4] In such applications thin layers of material are required which must be highly uniform and free of defects.

Several methods for the fabrication of zeolite thin films have recently been reported.[3] A common route used to produce membranes for gas separation involves zeolite crystallization onto a substrate (*e.g.* a porous ceramic) under *in situ* hydrothermal conditions. This method is generally satisfactory, although it has been difficult to control the membrane thickness and uniformity. In an attempt to overcome this problem, "secondary growth" methods are now being developed.[2,5,6] These involve two-stages (see Fig. 1). Firstly, zeolite is produced in a colloidal form by a hydrothermal reaction in the precursor solution. The colloidal zeolite particles are then separated and deposited on a substrate as a thin uniform layer. In a second stage this thin layer is then subjected to a further hydrothermal treatment. In this process the colloidal particles act as seeds for secondary growth, thus producing a uniform membrane layer. We have recently described[6] the synthesis of silicalite membranes using this method and demonstrated that their gas permeability is considerably higher than that achievable with membranes prepared by a one-step *in situ* crystallization of silicalite directly onto an alumina substrate.

In order to optimise the secondary growth route a better understanding of the first stage of the method is required. This includes (a) the process of zeolite colloid formation, and (b) the mechanism by which the colloidal particles are consolidated to give a continuous layer structure. An insight into both of these aspects has been achieved using small angle neutron scattering (SANS), as described here in studies of colloidal silicalite

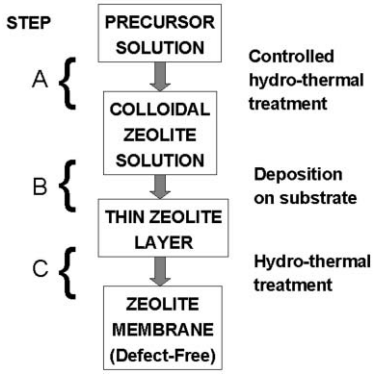

Fig. 1 Different stages in the "Secondary Growth Process" as used to synthesize zeolite membranes by the deposition of colloidal zeolite particles onto a substrate.

†Basis of a presentation given at Materials Discussion No. 5, 22–25 September 2002, Madrid, Spain.

DOI: 10.1039/b204171p

(MFI), prepared using similar procedures to those we have used above.[6] The SANS technique is particularly appropriate because it can be used for *in situ* measurements even under hydrothermal conditions, and also when the colloidal particle concentration is very high.[7,8]

Work on another zeolite system, zeolite A (LTA), will also be described. For this system the hydrothermal synthesis conditions have again been optimised so as to favour homogeneous nucleation and colloid formation. This has been achieved using precursor solutions of silicate and aluminate oligomeric species, which contain the tetramethylammonium organic cation (TMA); the latter acts as a structure directing agent. The mechanisms of interaction of these oligomeric species and TMA have recently been investigated by NMR measurements on solutions extracted during the first stage of the reaction using this preparative route.[9] Here we describe the application of small angle X-ray scattering (SAXS), and other techniques to determine the properties of colloidal species which form during subsequent stages of the reaction before the appearance of well-crystallized zeolite A.

Experimental

Silicalite-1 colloids were prepared using routes similar to that described previously by Schoeman and co-workers.[10,11] For the SANS investigations, the composition of the precursor solution was: $1SiO_2 : 4EtOH : 0.36TPAOH : 0.01NaOH : 19H_2O$. The kinetics of colloid formation at 363 K were followed by SANS measurements on this reaction solution at intervals over a period of approximately 22 hours. Other SANS measurements were made on a series of samples having a progressively increasing particle concentration, which eventually resulted in a solid phase. The size of the colloidal particles in this series corresponded to that after approximately 20 hours reaction time. A contrasting series of SANS measurements was also made on dilute dispersions of the same particles dispersed in different H_2O/D_2O mixtures to derive the scattering length density of the colloidal particles, as described previously.[12]

Zeolite A (series A) was prepared by the method described previously,[9] using a mixture of two solutions — one of an aluminate, the other a silicate. These two solutions were obtained by dissolution of ultrafine alumina and silica powders in solutions of tetramethylammonium hydroxide (TMAOH) under hydrothermal conditions. Using this mixture, having the composition: $1SiO_2 : 0.20Al_2O_3 : 3.2TMAOH : 0.08NaOH : 80NaOH$, the reaction was carried out at 353 K. Solid samples were extracted from the reaction mixtures, at periodic intervals during the course of the reaction, by ultracentrifugation (3×10^4 rpm for 15 minutes, corresponding to a relative centrifugal field, RCF_{max}, of $\sim 9 \times 10^4$ g). These samples were then washed several times (by redispersion in water and recentrifugation until the pH of the centrifugate reached ~ 9). The washed samples, after air-drying, were then characterised by XRD and SAXS. The surface and porous properties were also determined from nitrogen adsorption isotherms, measured at 77 K, on samples after outgassing at 523 K.

Zeolite A (series B) colloids with an approximate size of 300 nm were also produced from another prehydrolysed solution containing silicate and aluminate oligomers with a different composition: $1SiO_2 : 0.59Al_2O : 2.6TMAOH : 0.25NaOH : 100H_2O$. This precursor solution was heated at 353 K for 72 hours. Colloidal zeolite was extracted from the milky solution by centrifugation. The product was redispersed in water and centrifugations repeated until the pH of the colloidal dispersion was 10.3.

SANS measurements were made at the Institut Laue Langevin, Grenoble, using the small angle scattering instrument, D22, as described previously.[13] Measurements were made in the momentum transfer range, Q, of 2.10^{-3} to $>2.5.10^{-2}$ Å^{-1}, where $Q = 4\pi\sin\theta/\lambda$, and λ is the neutron wavelength.

SAXS measurements were performed in the range $8 \times 10^{-4} < Q < 0.1$ A^{-1}, using a high-resolution Bonse–Hart camera, fitted with two pairs of channel-cut germanium crystals, as described previously.[14] A rotating anode X-ray source with a copper target was employed.

Zeolite samples were characterized by SEM and XRD as previously.[15]

Measurements of nitrogen adsorption isotherms (77 K) were made volumetrically (Micromeritics, Digisorb).

Theory

A brief outline of the theory of small angle scattering from colloidal particle systems will be given here. In particular we will consider SANS, as it is applied more specifically to characterize silicalite sols and their interactions. Further details of SANS and the analysis of particle systems has been reported elsewhere.[8,16,17]

The intensity of neutrons scattered at small angles, $I(Q)$, from a dilute system of non-interacting particles is given by:

$$I(Q) = V_p^2 n_p (\rho_p - \rho_s)^2 P(Q) \quad (1)$$

where V_p and n_p are respectively the volume and number concentration of particles, ρ_p and ρ_s are the respective scattering length densities of the particles and solvent, and $P(Q)$ is a particle form factor. The momentum transfer, Q, is defined by

$$Q = 4\pi\sin\theta/\lambda \quad (2)$$

where θ and λ are the scattering angle and wavelength of radiation employed.

The form factor has been evaluated for a variety of particle shapes (spheres, rods, discs *etc.*). However, in the range of very low Q its form can be generalized for all particle shapes by use of the Guinier approximation:

$$P(Q) \approx \exp(-Q^2 R_g^2/3) \quad (3)$$

where R_g is the radius of gyration of the particles. For spheres, an approximation used for the silicalite particles is $R_s = 1.29R_g$, where R_s is the sphere radius.

From eqn. (1) it is seen that the scattered intensity is determined by the particle/solvent contrast factor, given by $(\rho_p - \rho_s)$.[2] The solvent contrast has been varied here by using appropriate mixtures of H_2O and D_2O to determine the "matching" condition.

In more concentrated dispersions, the intensity distribution is modified by the effects of interference, which depend on the spatial ordering of the particles. The scattered intensity is then

$$I(Q) = V_p^2 n_p (\rho_p - \rho_s)^2 P(Q) S(Q) \quad (4)$$

where $S(Q)$ is the static structure factor, which is determined by the nature of the interaction potential; for non-interacting systems $S(Q) = 1$. The spatial distribution of the particles as a function of the mean interparticle separation, r, is given by the particle pair-distribution function $g(r)$ and is related to $S(Q)$ by the Fourier transform

$$g(r) = 1 + \frac{1}{2\pi^2 n_p} \int_0^\infty [S(Q) - 1] Q^2 \frac{\sin Qr}{Qr} \mathrm{d}Q \quad (5)$$

Structural changes which occur during the progressive concentration of sols into gels and porous solids have been analysed previously on this basis.[8] In the present investigation such

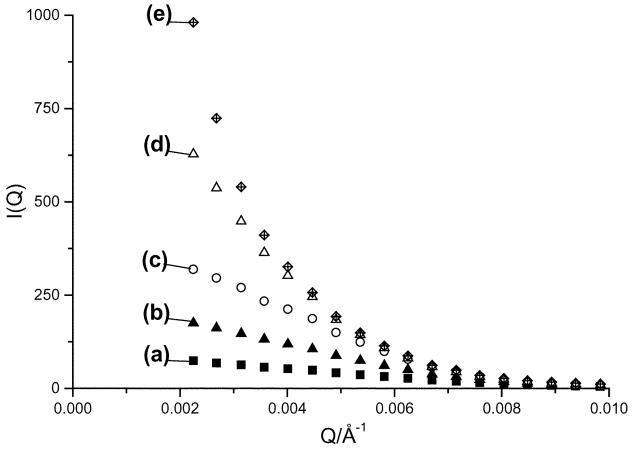

Fig. 2 Kinetic evolution of SANS during the hydrothermal (363 K) synthesis of colloidal silicalite-1. After, (a) 18, (b) 19, (c) 20, (d) 21, and (e) 22 h.

Table 1 Radii of gyration, R_g, and equivalent sphere radii, R_s, of silicalite colloids as determined from SANS at different times during the hydrothermal synthesis reaction

Synthesis time/h	R_G/nm	R_S/nm
18	29.2	37.5
19	33.0	42.6
20	35.0	45.5
21	42.3	54.5
22	45.1	58.5

structuring and short-range ordering is typified by distinct maxima in $S(Q)$ from which the interparticle separation, r, can be estimated.

Results and discussion

Silicalite-1

The evolution of the SANS during hydrothermal treatment (363 K) of the silicalite-1 precursor solution is shown in Fig. 2. This illustrates that the scattered intensity, $I(Q)$, was hardly significant during an induction period of nearly 18 hours. Thereafter, $I(Q)$ increased rapidly, corresponding to the formation and progressive growth of colloid particles. The size of the particles corresponding to each curve (corresponding to a counting time of $\sim$3 minutes) was derived from Guinier plots as given in Table 1. The quality of the fits of the experimental

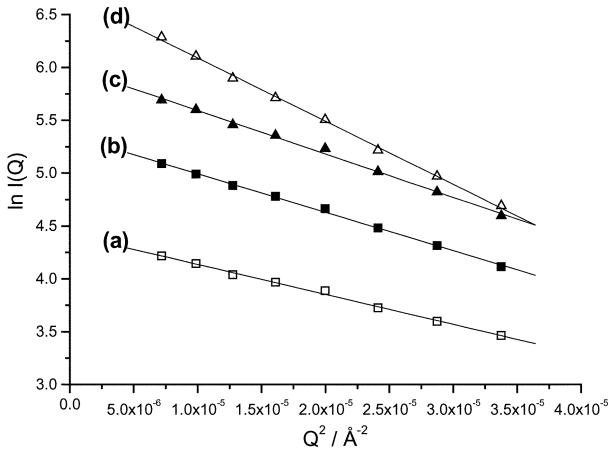

Fig. 3 Guinier plots of SANS for colloidal silicalite-1 after different synthesis times at 363 K. (a) 18, (b) 19, (c) 20, and (d) 21 h.

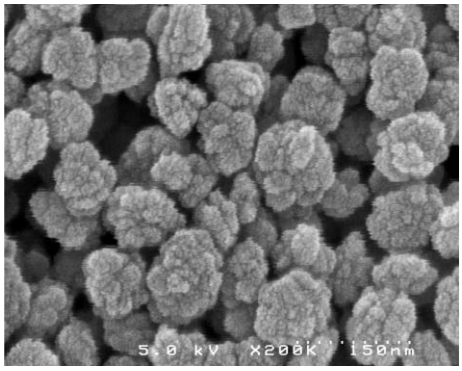

Fig. 4 SEM of colloidal silicalite-1 particles.

data to the Guinier relationship (*cf.* Fig. 3) were good, indicating a narrow particle size distribution in each sample.

SEM results also confirmed that the particles were approximately spherical and of uniform size, as illustrated in Fig. 4 for a sample extracted after 20 hours. Here the particles have diameters in the range from $\sim$85 to $\sim$95 nm, which is in close accord with the SANS results. At higher resolution it is evident however that the particles have a "cauliflower-like" appearance and seem to be formed by clusters of much smaller sub-units. The size of these sub-units appears to be less than 4 nm, and is at the limit of resolution of the SEM technique.

From a further analysis of the evolution of the series of SANS curves in Fig. 2, a tentative mechanism for the nucleation and growth of colloidal particles can be proposed. Thus from eqn. (1) it is evident that $I(Q)_{Q\rightarrow 0}$ will be dependent both on the particle number concentration, n_p, and the particle volume, V_p, according to the following relationship:

$$I(Q)_{Q\rightarrow 0} \propto n_p V_p^2 \propto n_p R_s^6 \quad (6)$$

This assumes that the particles remain uniform in size during the growth process and are spherical, with a diameter R_s. Both of these conditions are reasonably satisfied here. Furthermore, if we assume a process of sudden nucleation and rapid growth, with no further formation of additional nuclei, then $I(Q)_{Q\rightarrow 0} \propto R_s^6$. The good agreement to this relationship is demonstrated by the linearity in Fig. 5 covering the reaction from 18 to 22 hours. This suggests that colloid particles are formed after an induction time by the rapid clustering of sub-units; these particles subsequently grow by further accretion of sub-units which exist in solution.

Further insight into the internal structure of the colloidal particles was obtained from measurements of SANS under

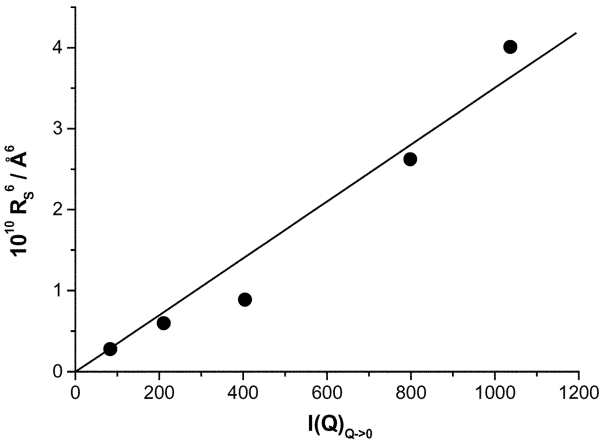

Fig. 5 Dependence of R^6_s *vs.* $I(Q)_{Q\rightarrow 0}$ for colloidal silicalite-1 after different synthesis times at 363 K. Points corresponding to increasing R_s are for synthesis times of 18, 19, 20, 21, and 22 hours respectively.

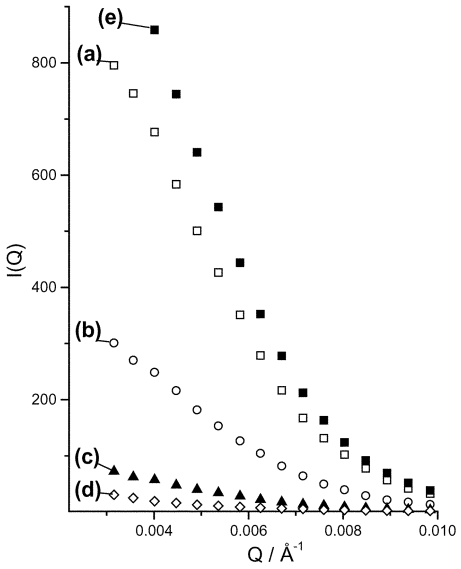

Fig. 6 SANS of colloidal silicalite-1 showing the effect of contrast variation by dispersion in different H_2O/D_2O mixtures. D_2O concentrations (% v/v) are: (a) 17, (b) 30, (c) 40, (d) 50, and (e) 66.

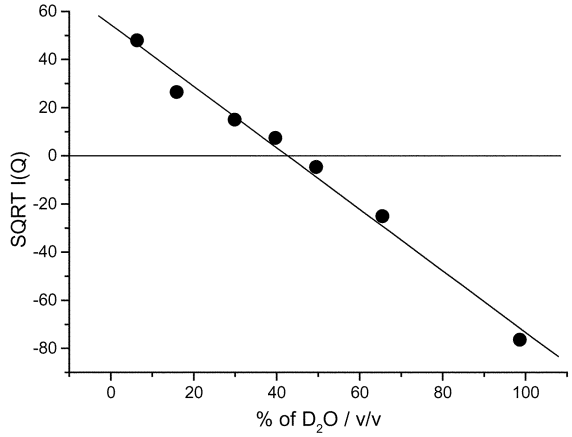

Fig. 7 Contrast matching plot for colloidal silicalite-1.

different particle/solvent contrast conditions. Such contrast variation measurements were made with a dilute particle dispersion of the same concentration in a series of different H_2O/D_2O mixtures, as previously described.[12,18] The samples were prepared from a colloidal dispersion in pure D_2O which had formed after approximately 20 hours under the same synthesis conditions as above. This reference dispersion in D_2O was concentrated by ultracentrifugation. Using this stock solution, a series of appropriate mixtures containing D_2O and H_2O was prepared by dilution with H_2O, and further exchange procedures. The effect of solvent contrast on the SANS for some of these mixtures is illustrated in Fig. 6. It will be noted that these all have the same form but vary considerably in relative intensity. The contrast matching condition was obtained from a plot of $[I(Q)_{Q\rightarrow 0}]^{1/2}$ *vs.* D_2O volume fraction as shown in Fig. 7. This plot is linear, in accord with the relationship in eqn. (1) above. The scattering length density of the particles, ρ_p, can therefore be derived from the zero intensity intercept where ρ_p and ρ_s are identical. The value of ρ_s for an aqueous solvent for this composition (*viz.* containing 42.5% v/v D_2O) is 2.38×10^{10} cm^{-2}. This compares with that of 3.47×10^{10} cm^{-2} for amorphous silica, having a mass density of 2.20 g cm^{-3}. The corresponding "effective" density of the silicalite particles as derived from their scattering length density in solution is therefore 1.51 g cm^{-3}. This value is considerably smaller

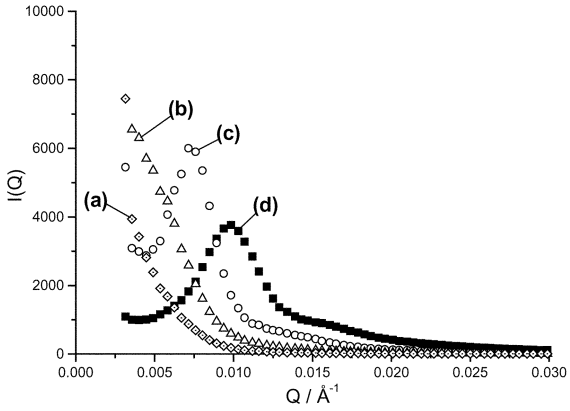

Fig. 8 SANS of colloidal silicalite particle dispersions showing effects of increasing volume fraction (particle diameters are approximately 80 nm). Particle volume fractions, Φ, are: (a) 0.02, (b) 0.05, (c) 0.15, and (d) dried solid.

and may reflect a more open structure of the particles which are formed by packing of the sub-units. A more quantitative analysis should take account of the unit cell dimensions of the silicalite sub-units and the possible effects of any tetrapropylamine occluded in the structure. If it is assumed that the unit cell structure and composition of these sub-units is the same as in well crystallized silicalite, which has an orthorhombic structure containing four TPA molecules per unit cell,[19] then one obtains a density of 1.86 g cm^{-3}. This calculation is based on a structure which contains TPA but not water. The effective density of the hydrated sub-units could therefore be greater than this. Such an analysis therefore remains tentative, but it can be concluded that the low density for the colloidal particles as determined by the contrast matching experiment, cannot be fully accounted for unless the particles have a somewhat "open" structure formed by the packed sub-units.

SANS measurements were also made on a series of samples of increasing colloid concentrations to obtain an insight into the mechanism by which the particles give rise to a consolidated layer structure. Results in Fig. 8 are for particles formed after approximately 19 hours reaction. (The salt concentration of the colloidal particle dispersions was reduced by repeated centrifugation and exchange of the supernatant solution with deionised water; dispersions of increasing concentration were prepared from the deionised reference sample by controlled centrifugation procedures). At the lowest volume fraction, ϕ, of 2%, the form of the scattering is similar to that in Fig. 2, corresponding to non-interacting particles with a diameter of $\sim$83 nm. However, as the concentration is increased there is evidence of interference in the SANS. This is evident in the pronounced maximum which occurs at $Q \sim 8 \times 10^{-3}$ Å^{-1} for the dispersion with $\phi = 15\%$. This feature can be ascribed to an ordering of the particles due to inter-particle repulsion forces as discussed earlier above. Such effects have already been described in detail for sol–gel particle systems, such as silica, ceria[8] and clay particle dispersions[20] for example. The position of this maximum corresponds to an approximate inter-particle spacing of 80 nm. This distance is similar to the particle diameter and thus implies that the particles are in contact.

For the solid phase (as formed as a thin layer by slow drying of the dispersion on a substrate), the position of the interference peak is shifted to a higher Q of 0.010 Å^{-1}, indicating a closer particle separation of approximately 63 nm. This separation is smaller than the apparent particle diameter, which tentatively suggests that some inter-penetration or coalescence of the colloid particles occurs. It is also evident that the zeolite particles in the solid layer have a high packing density and short-range order. Such an ordered arrangement of particles is apparent both from the marked interference peak and also the secondary maximum in the SANS curve at $Q \sim 0.018$ A^{-1}

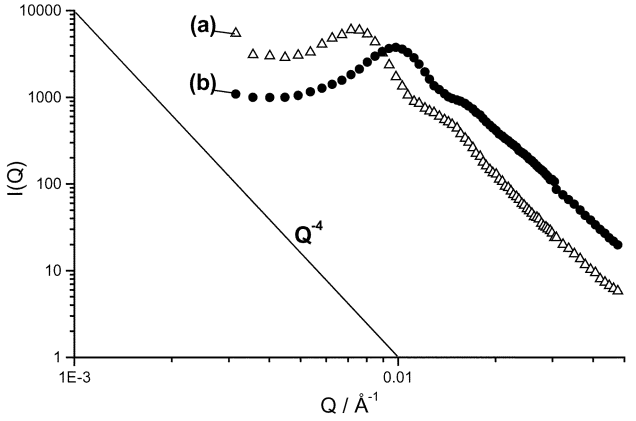

Fig. 9 SANS of colloidal particles of silicalite, (a) in a concentrated dispersion (volume fraction 0.15) and (b) when formed as a dried deposited layer.

as shown in Fig. 9. The initial formation of such a compact structure may indeed be important in the subsequent secondary growth process employed to produce defect-free zeolite membranes.

Zeolite LTA

The development of zeolite LTA was investigated during the course of hydrothermal reactions at 353 K in solutions with composition A. At this temperature the mixtures of the solutions of aluminate and silicate precursors remained transparent for approximately 10 hours. Thereafter the reaction mixture became opalescent and then increasingly opaque indicating the existence of colloidal particles with a size considerably larger than 10 nm. (In dispersions containing colloids with a size <30 nm Rayleigh light scattering occurs. This is of very low intensity and consequently dispersions may appear visually transparent). At progressive times during the reaction, the solid colloid phase was extracted from the reaction solutions by ultracentrifugation, using the procedure described above. These solid samples (after washing, recentrifugation and air drying) were characterised by XRD, SAXS and nitrogen adsorption measurements, as described below.

From the XRD time series in Fig. 10 it is evident that there is a long induction period. During this period, a very broad diffraction feature at $2\theta \sim 30^\circ$ is evident (Fig. 11a) this can be ascribed to an amorphous silicate phase. The first significant evidence of a crystalline phase occurs after 54 hours, when broad diffraction lines appear. After 60 hours the diffraction pattern has developed further — the lines become narrower and more intense, and correspond to a crystalline LTA structure. This crystallization process continues and, at 72 hours, from the lines as indexed, it is evident that only zeolite LTA is present.

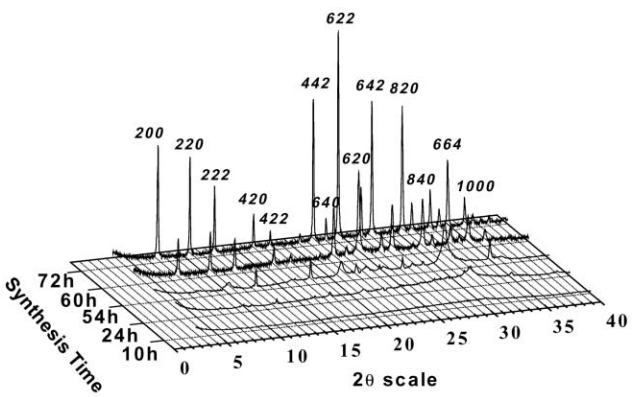

Fig. 10 X-Ray diffraction profiles of samples produced after different times in a zeolite LTA synthesis mixture at 353 K. After 72 hours, all the peaks can be indexed to the LTA structure as shown.

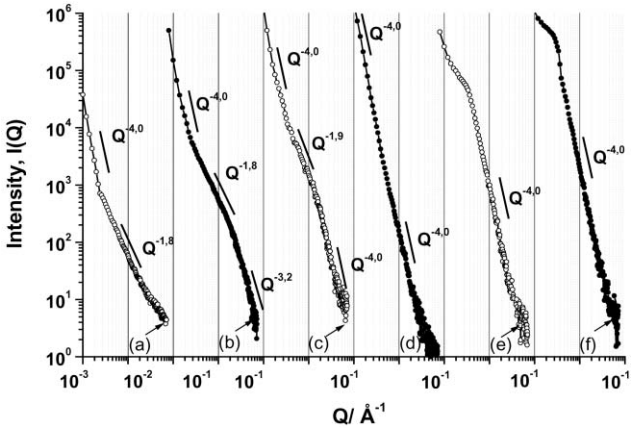

Fig. 11 SAXS of samples produced after different times in a zeolite LTA synthesis mixture at 353 K. Reaction time: (a) 2, (b) 10, (c) 20, (d) 48, (e) 60, and (f) 72 h. N.B. The origin for the Q axis is 10^{-3} Å^{-1} and data for each sample after (a) are displaced successively by two decades for clarity.

The SAXS of a series of samples extracted during the induction period and at the first stages of the crystallization process is shown in Fig. 11. For the transparent "glassy" material formed after 2 hours (Fig. 11a), the SAXS intensity is relatively weak. Two power law regions can be defined. At low Q ($<3 \times 10^{-3}$ Å^{-1}), Porod scattering occurs, where $I(Q) \propto 10^{-4}$. This corresponds to scattering from large objects, with dimensions considerably greater than the inverse Q space (*viz.* $\gg 10^3$ Å). This can be ascribed to the granular structure of the powder samples. In the higher Q region the power law decay of $Q^{-1.8}$, which extends to $> 2 \times 10$ Å^{-1}, can be tentatively ascribed to mass fractal scattering from aggregates of much smaller particles (<100 Å). After 10 hours (Fig. 11b) the SAXS intensity has increased. The Porod scattering at low Q is still evident. This is again followed by a region of lower slope, and then an inflexion is evident, at $\sim 3 \times 10^{-2}$ Å^{-1}, followed by a decay of approximately $I(Q) \propto Q^{-3.2}$ These features are in accord with the growth of the small particles, which now also exhibit surface fractal scattering in the high Q range. This trend continues up to 20 hours (Fig. 11c) however the inflexion has now shifted to a lower Q of approximately 2×10^{-2} Å^{-1} , indicating further growth in the particles. Furthermore, the decay in the high Q region is now close to Porod in character (Q^{-4}), indicating a more "smooth" or less fractal particle surface.

After 48 hours (Fig. 11d) it appears that a shift in the inflexion to even lower Q occurs. The inflexion is thus obscured, as it overlaps with the strong Porod scattering due to the granular texture of the sample. The subsequent evolution of the SAXS indicate that changes in this texture occur during the initial stages of zeolite crystallization. This is illustrated after 60 hours (Fig. 11e) and 72 hours (Fig. 11f) by the suppression of the Porod scattering in the very low Q range. The SAXS can now be ascribed to a single particle component, which corresponds to the discrete zeolite crystals. The inflexions in the SAXS at much lower Q (~ 2–3×10^{-3} Å^{-1}) indicates that the size of these crystals is considerably larger than the particles which are present during the induction period. An approximate size of 0.2 μm can be tententatively estimated from the position of these inflexions.

An indication of the size of the primary particles which are present during the induction period can also be obtained from the positions of the inflexions observed in the SAXS after 10 and 20 hours (*viz.* at approximately 3 and 2×10^{-2} Å^{-1} respectively). These correspond to sizes of 20 and 30 nm respectively. These sizes can be compared with the corresponding

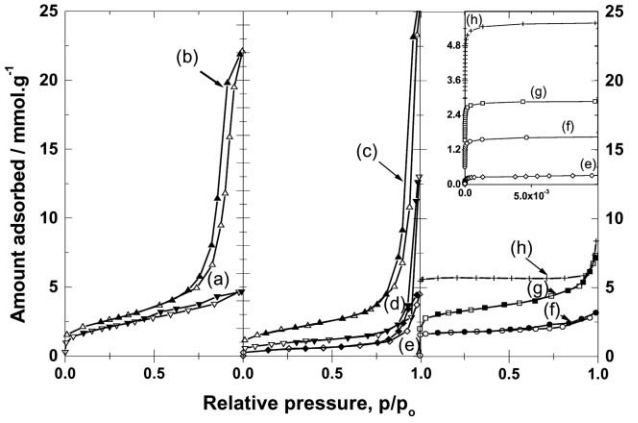

Fig. 12 Adsorption isotherms of nitrogen at 77 K for samples produced after different times in a zeolite LTA synthesis mixture at 353 K. Synthesis times are: (a) 2, (b) 8, (c) 10, (d) 20, (e) 54, (f) 60, (g) 72 h, and (h) >1 week. N.B. Open symbols adsorption; closed symbols desorption. Some points have been omitted for clarity. Inset shows the low-pressure region of the isotherms.

radii of gyration, R_g, of 13 and 15 nm, as obtained from the respective Guinier plots. The accord is not unreasonable considering the limitations in the application of the Guinier method here (*viz.* restricted Q range due to overlapping Porod scattering at $Q < 10^{-2}$ Å^{-1}, and possible interference effects due to multiple particle scattering). Because of the overlapping low-angle Porod scattering, this procedure can not be extended to an analysis of the SAXS after 48 hours.

From measurements of nitrogen adsorption isotherms it is also possible to obtain an indication of the size of the primary particles, and furthermore the porous structure which results when they are consolidated during the process of ultracentrifugation. First we will consider the evolution and general characteristics of the isotherms at different stages of the reaction as illustrated in Fig. 12. Thus after 2 hours (Fig. 12a) the isotherm is of type IV in the IUPAC shape classification,[21] the narrow hysteresis loop indicating the presence of a relatively small volume of mesopores with a size, r_p, covering a wide range (2 to 5 nm). Further analysis of this isotherm using the α_S method[22] indicates that the sample is also microporous (see Table 2). After 8 hours (Fig. 12b) the isotherm changes markedly. It still has a type IV form, but it is evident that the mesopore volume has increased markedly and the size is now more uniform (*cf.* Table 2). Such an isotherm is consistent with an open porous structure formed by the packing of "globular" shaped particles, as has been discussed previously.[22–24] The surface area is related inversely to the size of the particles, and the pore diameter, the dimensions of the throats connecting the interstices in the packed structure. Such a model is in accord with the evolution of the isotherms after 10, 20 and 54 hours respectively (Fig. 12c–e). From these it is evident that a progressive decrease in the surface area occurs in parallel with a corresponding increase in the pore diameter (Table 2). Such changes indicate a growth of the globular particles, as already evidenced from the SAXS. Furthermore, the decrease in pore volume noted after 20 hours may indicate a closer packing or some coalescence between the particles.

A striking change in the isotherms is noted between 54 and 60 hours (Fig. 12f) at the onset of zeolite crystallization. This results from a marked increase in adsorption at low relative pressure ($p/p_0 < 10^{-3}$), corresponding to a volume filling process in the micropores of the zeolitic structure. With further development of crystallinity after 72 hours (Fig. 12g) this micropore volume increases further. However, the isotherm in Fig. 12g shows that adsorption continues beyond a p/p_0 of 0.1 until almost 1.0 with little evidence of hysteresis. This continued uptake can be ascribed to adsorption on the external surface of the small zeolite crystals which have formed. In effect Fig. 12g can be considered as a composite isotherm of type I and type II. (N.B. type I and type II isotherms are associated with a microporous solid and a non-porous powder respectively[21]). Composite isotherms with these features have been discussed in detail by Gregg and Sing[22] and have been reported previously for microporous oxides and carbons by others.[25,26] The usual isotherms reported for zeolites are of type I, as shown in Fig. 12h. This corresponds to another sample of zeolite LTA, consisting of much larger crystals in the micron size range, prepared using the same recipe, but after considerably longer hydrothermal treatment. It will be noted that the micropore volume of this sample is fully developed and in accord with that expected for zeolite LTA (see Table 2). The development of the intracrystalline microporosity is illustrated by the inset in Fig. 12, which shows the adsorption of nitrogen at very low p/p_0 for the samples just before and after the onset of crystallisation.

The structure of thin layers formed by the deposition of zeolite A particles from solutions of low ionic strength was also investigated by SEM. These studies were made with samples prepared using the composition of series B. After 72 hours hydrothermal reaction at 353 K, SEM showed approximately spherical particles with a diameter of ~320 nm had formed.

When a colloidal dispersion in water was dried on a substrate a uniform layer of particles was formed as illustrated in Fig. 13. Here the substrate is an anodic alumina membrane disc (Anopore™, Whatman, UK) with a nominal pore size of 200 nm. It will be noted that the zeolite layer has a uniform thickness of ~10 μm and that the packing of the colloidal particles is efficient and regular. The latter features have already been shown to occur in the dried layers formed from silicalite particles, where SANS has provided an indirect although more quantitative indication of the structure of the consolidated particle structure.

Conclusions

In this paper we have described an investigation of the synthesis of two zeolite systems, silicalite-1 and zeolite LTA, in which colloidal particles are formed in solution under hydrothermal

Table 2 Surface and porous properties of zeolite LTA precursor samples extracted from synthesis solutions after different times of reaction. N.B. The particle diameters are derived from specific surface areas assuming globular particles having a density of 2.2 g cm^{-3}

Sample	1	2	3	4	5	6	7	8
Reaction time/hours	2	8	10	20	54	60	72	>1 week
Specific surface area, A_s/m^2 g^{-1}	152	196	130	74	30			
Total pore volume[a], V_p/cm^3 g^{-1}	0.16	0.77	0.89	0.45	0.16	0.11	0.15	0.18
Pore diameter, d_p/nm	3–10	14	26	>60	>60	<2	<2	<2
Particle diameter[b], D_p/nm	8	13	16	21	41			
Micropore volume, V_m/cm^3 g^{-1}	0.08	0.08	0.08	0.04	0.03	0.06	0.11	0.18
Porosity, ε	0.26	0.63	0.66	0.5	0.26			

[a]V_p is the total pore volume derived from adsorption at $p/p_0 \approx 0.98$. [b]D_p is the equivalent particle diameter derived from As, assuming globular particles of density 2.2 g cm^{-3}.

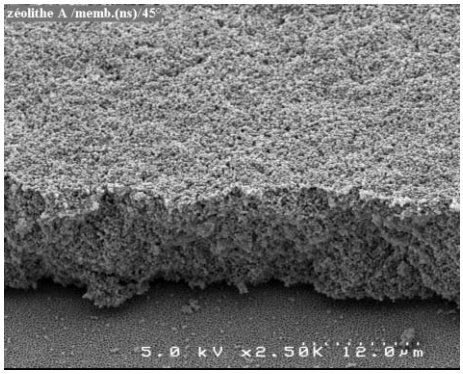

Fig. 13 SEM of layer of zeolite A particles deposited on an Anopore® alumina membrane support.

conditions. Colloidal particles of these two types of zeolite are important as precursors in the fabrication of membranes using the secondary growth process as earlier described. It is shown that for both of these zeolite systems, colloidal particles of sub-micron size can be formed after prolonged hydrothermal treatment at relatively modest temperatures. These particles can be further consolidated as thin layers by deposition from solution onto a substrate. The regularity in the particle packing is an important feature in the subsequent secondary stage of zeolite growth to give a defect-free layer, although this aspect has not be studied here.

An insight into the mechanisms of nucleation and growth of the zeolite particles can be tentatively inferred from these investigations. Such an aspect is of long-standing interest and has been considered previously by many workers.[27–29] It should however be noted that for the two systems which have been investigated here, the synthesis procedures both employ large concentrations of organic structure directing cations (tetra-propylamine and tetramethylamine) in solution. The role of these organic cations may indeed be important, as discussed by Schoeman and others[27,28] and therefore the mechanisms proposed may not be general for other systems using different precursors.

Firstly we consider silicalite-1 formation. Evidence from the SANS shows that after a long induction period of almost 18 hours, there is a rapid increase in scattered intensity. This increase can be ascribed to the rapid formation and growth of colloidal particles by a process of accretion of much smaller sub-units from solution. Both the SEM results and contrast matching measurements support such a particle structure formed from smaller units. The size of these sub-units appears to be close to 4 nm but is difficult to determine from SEM because it is at the limit of resolution of the technique. For such a small size, at the particle volume fraction used here, the SANS would be almost insignificant compared to the scattered intensity observed for the colloidal clusters which have a size approaching 100 nm. We note that the existence of very small units in precursor solutions of silicalite-1 has been proposed by Martens and co-workers.[30] These workers indeed propose that such units exist as "nano-blocks" with a defined size of 4 × 4 × 1.3 nm. From our investigations there is no evidence for such a precise size, although the range is similar to that inferred from SEM.

For the zeolite-A system we only have indirect evidence on the nature of the colloidal particles in solution, from the characteristics of the samples extracted by ultracentrifugation at progressive stages of the reaction. However, there is a general accord from SAXS, nitrogen isotherms and XRD for the existence of amorphous colloidal particles in solution during the induction or pre-cystallization stage (*viz.* between 8 and 54 hours). These particles appear to be "globular" in shape and grow in size as the reaction proceeds. The growth process may arise from the uptake of silica-aluminate oligomeric species from solution. Although there is no evidence available here to support this, the existence of such species has been shown from NMR measurements[9] made on solutions at the earliest stages of reaction, prior to particle formation. After 54 hours, the nucleation of a zeolite phase may occur within these globular particles. Such a process takes place in parallel with the continued growth of the particles, as indicated by SAXS. After 72 hours the particles have a size of approximately 300 nm, and appear from XRD to be crystalline. However, when compared with a sample prepared after much more prolonged hydrothermal treatment (>1 week), composed of well-defined cubic crystals, it is noted that the zeolitic microporosity is still not fully developed and that there is significant XRD line-broadening. Thus the mechanism of zeolite LTA formation is different from that proposed for silicalite. Nevertheless, in both cases such small partially crystallized zeolite particles can be packed in as ordered layers, as shown here. Furthermore, such consolidated particle structures may be labile in a secondary growth step to give inter-grown continuous zeolite layers.

Acknowledgements

We are indebted to Dr A. van der Lee for assistance with XRD measurements, to Mr El Mansouri for the measurements of nitrogen adsorption isotherms and Mr G. Nabias for SEM determinations. Access to neutron scattering facilities at the Institut Laue Langevin, Grenoble, is also gratefully appreciated. S. K. acknowledges financial support from the European Community under the Industrial and Materials Technologies Programme (contract no. BRPR-CT96-313).

References

1 R. M. Barrer, *Zeolites and Clay Minerals as Sorbents and Molecular Sieves*, Academic Press, New York, 1978.
2 M. Tsapatis and G. R. Gavalas, in *MRS Bulletin 24, Membranes and Membrane Processes*, ed. V. N. Burganos, Mater. Res. Soc., N.Y., 1999, p. 30.
3 J. D. F. Ramsay and S. Kallus, in *Recent Advances in Gas Separation by Microporous Membranes*, ed. N. K. Kanellopoulos, Elsevier, Amsterdam, 2000, pp. 373–396.
4 G. Cho, J. S. Lee, D. T. Glatzhofer, B. M. Funf, W. L. Yan and E. A. O'Rear, *Adv. Mater.*, 1999, **11**, 497.
5 L. C. Boudreau, J. A. Kuck and M. Tsapatis, *J. Membr. Sci.*, 1999, **152**, 41–59.
6 C. Algieri, G. Golemme, S. Kallus and J. D. F. Ramsay, *Microporous Mesoporous Mater.*, 2001, **47**, 127–134.
7 W. H. Dokter, T. P. M. Beelen, H. F. Garderen, R. A.van Santen and J. D. F. Ramsay, *Colloids Surf.*, 1994, **85**, 89–95.
8 J. D. F. Ramsay, *Chem. Soc. Rev.*, 1986, **15**, 335–371.
9 S. Smaihi, S. Kallus and J. D. F. Ramsay, *Studies in Surface Science and Catalysis*, **vol. 135**, eds. A. Galarneau, F. Di Renzo, F. Fajula and J. Vedrine, Elsevier, Amsterdam, 2001, p. 189.
10 A. E. Person, B. J. Schoeman, J. Sterte and J. E. Otterstedt, *Zeolites*, 1994, **14**, 557.
11 J. Hedlund, S. Mintova and J. Sterte, *Microporous Mesoporous Mater.*, 1999, **28**, 185.
12 J. D. F. Ramsay, S. W. Swanton, A. Matsumoto and D. G. C. Goberdhan, *ACS Advances in Chemistry Series, 234*, Am. Chem. Soc., Washington D.C., 1994, pp. 67–82.
13 *ILL Yellow Book, Guide to Neutron Research Facilities at ILL*, ILL, Grenoble, 2001.
14 Ph. Dieudonné, P. Delord and J. Phalippou, *J. Non-Cryst. Solids*, 1998, **225**, 220–225.
15 S. Kallus, P. Langlois, G. E. Romanos, Th. Steriotis, E. S. Kikkinides, N. K. Kanellopoulos and J. D. F. Ramsay, in *Studies in Surface Science and Catalysis*, **vol. 128**, eds. K. K. Unger, G. Kreysa and J. P. Baselt, Elsevier, Amsterdam, 2000, pp. 467–474.
16 A. Guinier and G. Fournet, *Small angle scattering of X-rays*, Wiley, New York, 1955.
17 J. D. F. Ramsay, *Adv. Colloid Interface Sci.*, 1998, **76**, 13–37.
18 J. D. F. Ramsay, R. G. Avery and L. Benest, *Faraday Discuss. Chem. Soc.*, 1983, **76**, 63.

19 M. M. J. Treachy and J. B. Higgins, *Collection of simulated XRD powder patterns*, 4th edn., Elsevier, Amsterdam, 2001; H. van Koningsfeld, H. van Bekkum and J. C. Jansen, *Acta Crystallogr., Sect. B*, 1987, **43**, 127–132.
20 J. D. F. Ramsay and P. Lindner, *J. Chem. Soc., Faraday Trans.*, 1993, **89**, 4207–4214.
21 J. Rouquerol, D. Avnir, C. Fairbridge, D. H. Everett, J. H. Haynes, N. Pernicone, J. D. F. Ramsay, K. S. W. Sing and K. K. Unger, *Pure Appl. Chem.*, 1994, **66**, 1739–1758.
22 S. J. Gregg and K. S. W. Sing, *Adsorption, Surface Area and Porosity*, 2nd edn., Academic Press, London, 1982.
23 J. D. F. Ramsay and R. G. Avery, *J. Colloid Interface Sci.*, 1973, **42**, 597–606.
24 J. D. F. Ramsay and B. O. Booth, *J. Chem. Soc., Faraday Trans. I*, 1983, **79**, 173–184.
25 S. J. Gregg and J. F. Langford, *J. Chem. Soc., Faraday Trans. I*, 1969, **65**, 1394.
26 J. D. F. Ramsay and R. G. Avery, in *Characterisation of Porous Solids*, eds. S. J. Gregg, K. S. W. Sing and H. F. Stoeckli, The Society of the Chemical Industry, London, 1979, p. 117.
27 B. J. Schoeman, *Microporous Mesoporous Mater.*, 1998, **22**, 9–22.
28 S. L. Burkett and M. E. Davis, *J. Phys.Chem.*, 1994, **98**, 4647.
29 M. Tsapatis, M. Lovallo and M. E. Davis, *Microporous Mater.*, 1996, **5**, 381.
30 C. J. Y. Houssin, B. L. Mojet, C. E. A. Kirschock, V. Buschmann, P. A. Jacobs, J. A. Martens and R. A. van Santen, in *Studies in Surface Science and Catalysis*, **vol. 135**, eds. A. Galarneau, F. Di Renzo, F. Fajula and J. Vedrine, Elsevier, Amsterdam, 2001, p. 140.